

# **Fabrication, Measurement and Verification of Switchable Dielectric Resonator Antenna Array for 5G Applications**

Nor Hidayu Shahadan  
Politeknik Ibrahim Sultan  
norhidayu@pis.edu.my

## **Abstract**

This paper describes the fabrication, measurement and verification of switchable dielectric resonator antenna array for 5G applications. 5G has a small size of antenna due to its shorter wavelength compared to the previous generation. This small size causes difficulty in obtaining precision in the fabrication process as well as measurement. In this research, the dielectric resonators (DR) are painstakingly aligned on the ground plane slot by using the tracing paper. This simple technique had successfully enhanced the accuracy of the DR position since the misalignment between the DR and the feeding network is minimized. The performance of the reflection coefficient of the fabricated antenna are verified by connecting the port directly to the Vector Network Analyzer (VNA) to minimal the additional losses during the measurement. The results of the reflection coefficient showed that the losses for five various switching angles have been reduced in the range of 2 to 3 dB. Subsequent to this, the switchable DRA array is able to steer at three various steering angle which are  $0^\circ$ ,  $-30^\circ$  and  $+30^\circ$  with 3dB beamwidth around  $24^\circ$ . Hence, the proposed switchable DRA array is capable to cover  $60^\circ$  sector which is considered suitable for 5G applications.

**Keywords:** dielectric resonator antenna, switchable antenna, antenna array

## **1.0 Introduction**

5<sup>th</sup> Generation (5G) has a variety of services and applications to complete the 4G technology and expected to be deployed beyond 2020 (Wang et al, 2014). It also draws attention to millimeter-wave bands with a frequency spectrum from 3 – 300 GHz that shrinks the wavelengths from 100 to 1 mm (Pi & Khan, 2011). With shorter wavelengths compared to the previous generation, more antennas can be packed into same area to compensate for the anticipated loss (Boccardi et al, 2014).

In this light, the dielectric resonator is proposed as the radiating element in the antenna design by considering its intriguing advantages such as wider bandwidth and lower loss compared to a microstrip patch antenna, thus, DRA is more suitable for higher frequencies applications (Nor et al, 2016). Even though the antenna gain and bandwidth can be enhanced using single element DRA design, however, it has a drawback in terms of capability of switching the direction beam. Then, the switchable DRA subarray is proposed in the improved design. This array consists of DR elements, driven element and parasitic elements. The parasitic elements are excited by the driven element through the mutual coupling and the phase shift between the elements can be adjusted by changing the value of the capacitor that is terminated at the parasitic elements.

The ECCOSTOCK HiK dielectric material with relative permittivity ( $\epsilon_r$ ) 10 and loss tangent ( $\delta_{tan}$ ) 0.002 is used as the prototype for DRs. Since the relative permittivity is inversely proportional to the impedance bandwidth, the proposed DRA is preferably using a small value of  $\epsilon_r$  at 10 in order to get a wider bandwidth. Nevertheless, the decreasing size of antenna in 5G has a

difficulty in obtaining precision in the fabrication process as well as measurement. The conventional method is less suitable for use in 5G technology as it will introduce losses in the measurement process (Yusuf & Gong, 2008). Therefore, an appropriate of the fabrication methods should be implemented in order to obtain accurate measurement results. Then, the performance of the reflection coefficient of the fabricated antenna can be verified using Vector Network Analyzer (VNA) while the antenna gain can be tested in an anechoic chamber (Shahadan et al, 2017).

In this paper, the simple fabrication and measurement technique are presented to show a better performance compared to the conventional techniques. As for the verification, the simulation for all designs are performed using Ansoft High Frequency Structural Simulator (HFSS) ver. 16.0 and while measurement is done using a vector network analysis (VNA) and tested in an Anechoic Chamber. The performance comparisons between simulated and measured results are also presented and discussed.

## 2.0 Substrate selection

Substrate selection is essential to ensure that the devices can satisfactorily operate at the designated frequency. Substrate plays an important role in antenna design and its selection depends on the operations' requirements. For this research, substrate selection is based on the dielectric constant, power loss, manufacturability and cost as listed in the data sheets produced by the manufacture (Rogers, 2016). Table 1 shows the properties of RT/Duroid 5880. It is composed by glass microfiber reinforced polytetrafluoroethylene (PTFE) for exacting stripline and microstrip circuit applications. Besides that, RT/Duroid 5880 substrate has a low dielectric constant that extends its usefulness at higher frequency design (8 GHz - 40 GHz) (Rogers, 2016).

**Table 1:** The properties of RT/Duroid 5880

Properties	Typical value
Dielectric Constant, $\epsilon_s$	2.2
Dissipation factor, $\tan \delta$	0.0009
Thermal coefficient of ( $ppm/^\circ C$ )	-125
Thermal conductivity ( $W/m/K$ )	0.20
Density ( $gm/cm^3$ )	2.2

Other than that, the substrate selection also takes into account achievement of the gain and directivity performance from the previous study. Research in (Ahmed et al, 2012) investigated the performance of the gain and the directivity in different substrate. It is clearly presented that RT/Duroid 5880 substrate offers highest gain and directivity better than Teflon substrate. Consequently, RT/Duroid 5880 with a dielectric constant ( $\epsilon_s$ ) of 2.2 was selected based on its performance and the capabilities in higher frequencies.

### 2.1 Performance of different RT/Duroid 5880 thickness

Prior to that, selection of an appropriate substrate thickness ( $t_s$ ) is one of important task in the antenna design. Accordingly, an investigation was done to the single element dielectric resonator antenna with the best feeding

technique (Shahadan et al, 2015) to identify the effect of varying the RT/Duroid 5880 substrate thickness. In this regard, the performances of the reflection coefficients, gain and directivity at 28 GHz were analyzed by varying the standard thickness,  $t_s$  at 0.127 mm, 0.254 mm, 0.381 mm and 0.508 mm as supplied provided by the manufacturers. As the thickness of the substrate decreased, surface wave and spurious feed radiation also decreased (Abdallah et al, 2017). Therefore, the thickness of the substrate should be kept as small as possible. From the Figure 1, it can be seen that RT/Duroid 5880 substrate with a thickness of  $t_s = 0.254$  mm produced the best performance in the reflection coefficient, gain and directivity at 28 GHz.

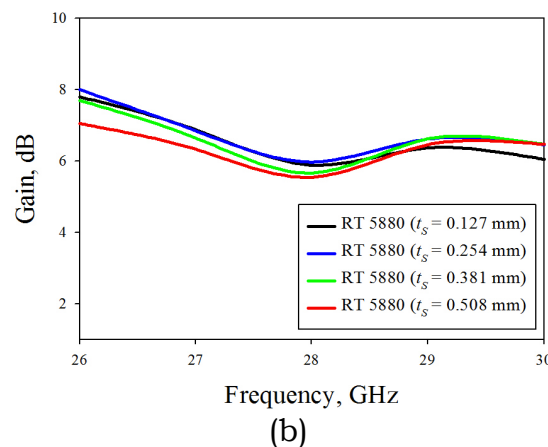
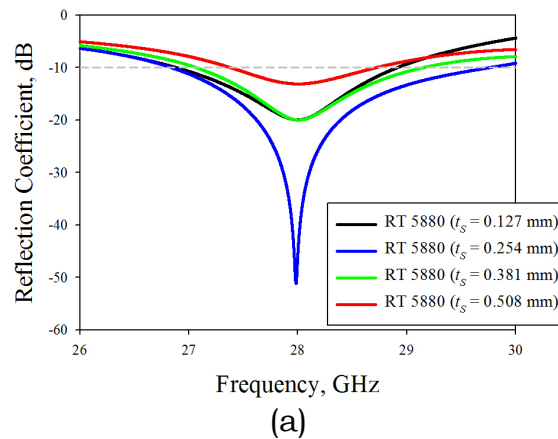


**Figure 1:** Simulated (a) reflection coefficients and (b) gain for different thickness of substrate

As for a preliminary study, single element DRA was investigated at 28 GHz in order to observe the antenna’s performance at higher frequencies. Furthermore, this frequency has been allocated in the Local Multipoint Distribution Service (LMDS) as a potential spectrum in future technology (Pi & Khan, 2011). In spite of that, frequency range of the antenna measurement facilities is limited up to 20 GHz, thereby, the onward DRA designs are stipulated at 15 GHz to facilitate an ideal fabrication and measurement processes. Moreover, as according to Ofcom, the spectrum bands above 6 GHz are also considered ideal for 5G applications and 15 GHz is one of the potential spectrum bands.

### 3.0 Antenna fabrication process

There are several processes involved for the proposed antenna to be built as a prototype. The design is printed on the transparency film and placed onto the board for laminating process before being exposed to the ultraviolet (UV) light. Then, the substrate board is submerged into a developer solution until the shape of a feeding structure can be seen. Next, the board is etched using chemical photoresist stripper to eliminate the unwanted copper from the plated board. Chemical Etching is at a higher precision level with less cost, shorter lead time, more design flexibility, and no need for deburring compared to CNC Machining. Figure 2 shows the fabrication process and the equipment used.

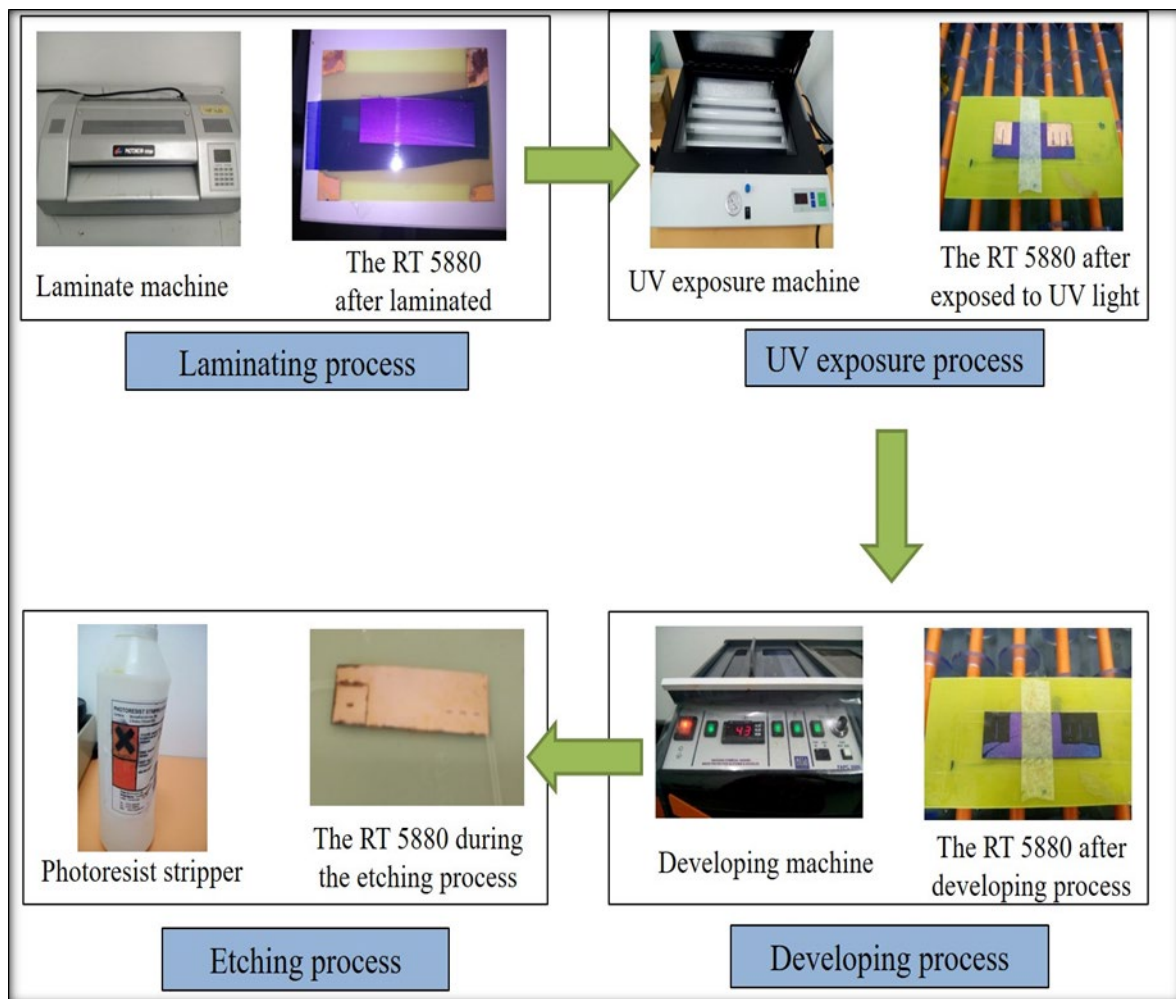


**Figure 2:** The antenna fabrication process

Meanwhile, the glue with thickness about 0.05 mm is used to attach the DR to the ground plane. In this regard, the surface of the ground plane must be properly cleaned to prevent any air gap formation between the DR and the ground plane. In this process, the DRs were painstakingly aligned on the ground plane slot by using the tracing paper as depicted in Figure 3. This enhances the accuracy of the DR position since the misalignment between the DR and the feeding network is minimized. In this regard, Microstrip Slot Aperture (MSA) is selected as a feeding structure due to its performance that fulfills the 5G requirements (Shahadan et al, 2015). The

advantage of having the feed network located below the ground plane is, it can avoid the spurious radiation from the feed thus reducing the interference from undesired directions. RF SMA Connector End Launch Jack that can operate up to 18 GHz is used to for feeding the DR antenna.

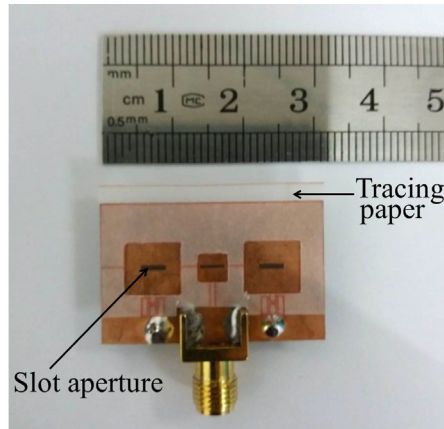


**Figure 3:** The process to attach the DR

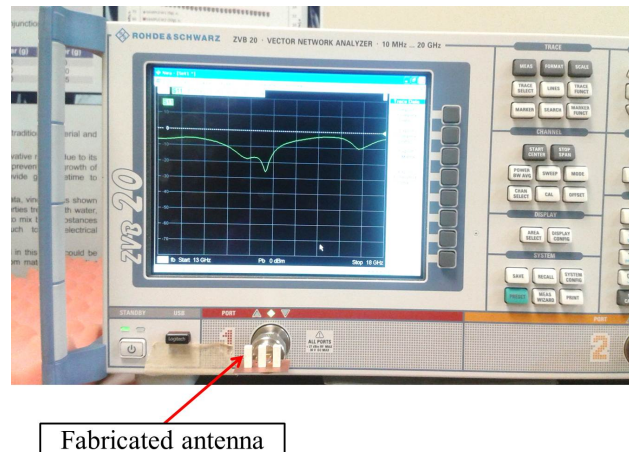


**Figure 4:** The S-parameter measurement using a VNA

#### 4.0 Antenna testing and measurement process

Several parameters need to be observed during verification process of the proposed antenna design. In this research, the most important results to be acquired are reflection coefficient, radiation patterns and gain. Therefore, the performance of the fabricated antenna design is indispensable to be measured, so that the comparison with the simulation result can be observed to ensure the performance of the antenna is as required. It started with a single element DRA design, followed by the switchable DRA subarray (3-elements) and lastly, the high-gain switchable DRA array (6-elements).

##### 4.1 Reflection coefficient measurement

Figure 4 shows the Rohde&Schwarz ZVB20 VNA that uses frequency range from 10 MHz to 20 GHz in obtaining the resulted reflection coefficient. The  $|S_{11}|$  specifications of the proposed antennas is as good as possible less than -10 dB within the operating frequency range to ensure the antenna has the maximum reflected power of 10% while 90% of power is being transmitted (Balanis, 2005). Besides, the 10-dB impedance bandwidth is

aimed to achieve more than 1 GHz as required in 5G applications (Pi & Khan, 2011).

The reflection coefficient is measured by connecting the proposed antenna to one of the provided ports in the VNA. There is a calibration process required prior to the  $|S_{11}|$  measurement. The calibration is conducted on one port calibration which is an open, short and load. In this light, the port is connected directly to the VNA to minimal the additional losses during the measurement. Since the measurement of radiation pattern and the antenna gain are also important instead of the  $|S_{11}|$ , thus, the following section explains these measurements of the fabricated antenna.

#### 4.2 Radiation pattern and gain measurement

In this research, the radiation pattern and gain of the fabricated antenna is measured in an Anechoic Chamber at Electromagnetic Compatibility (EMC) Lab of Universiti Tun Hussein Onn Malaysia (UTHM). The interior surface of the chamber is covered with the radiation absorbent material to prevent reflection of the electromagnetic waves. The measurement steps started with setting up the calibration that measures radiation pattern and gain of the antenna. For calibration purpose, two identical horn antennas are used. One of the horn antenna acts as the transmitter and another horn antenna referred as reference antenna that acts as the receiver. The reference antenna is then replaced with the proposed antenna as shown in Figure 5. The radiation pattern is automatically measured by rotating turning table at two planes which are  $E$  and  $H$ -plane at desired frequencies. Antenna in the horizontal condition is measured in getting the  $E$ -plane radiation pattern. Likewise, the vertical configured antenna is then tested for  $H$ -plane.

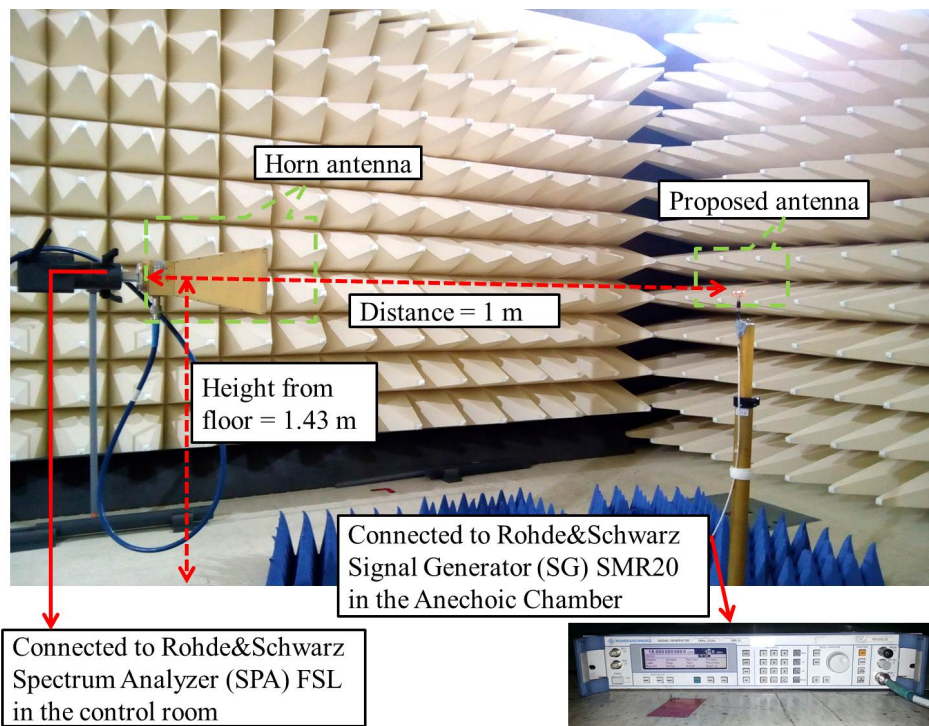


**Figure 5:** The setup for radiation pattern and gain measurement

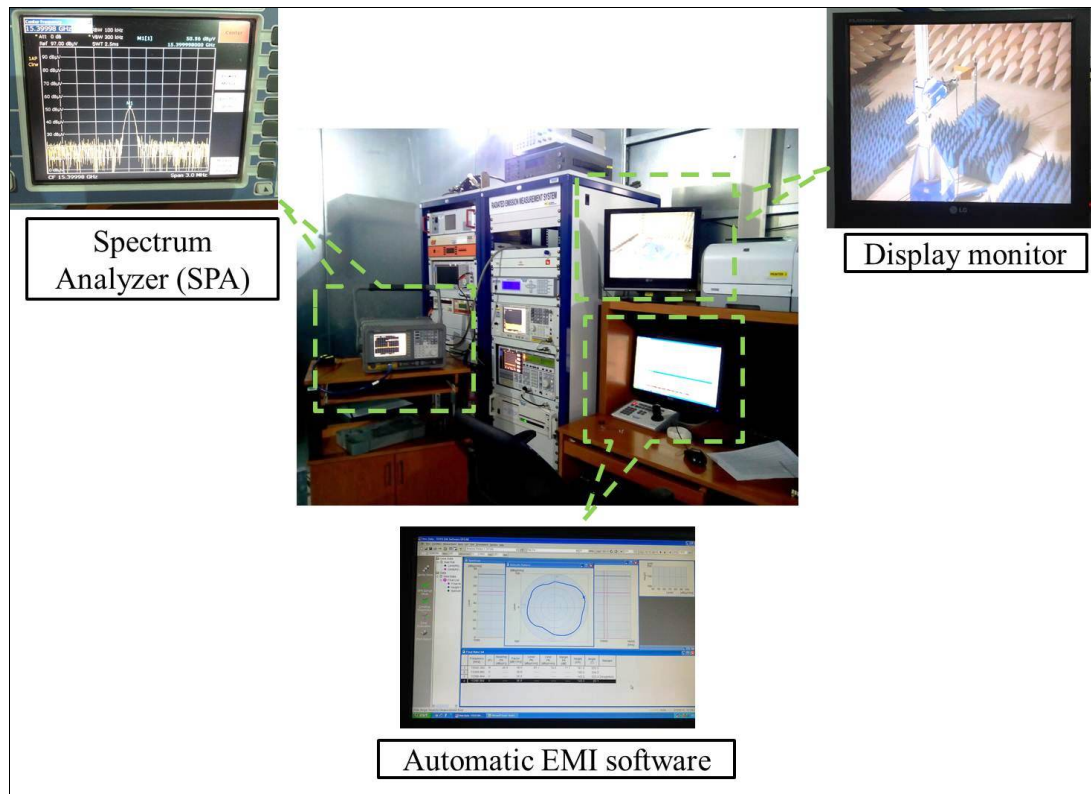


**Figure 6:** The control room setup

In the meantime, the measurement process can be monitored from the control room that is equipped with radiation emission measurement system complete with display monitor, spectrum analyzer and an Automatic EMI software as shown in Figure 6. During the measurement process, this software extracts all data and produce the results accordingly. In this case, the gain-transfer method is used to measure the gain of the proposed antenna (Balanis, 2005). This method utilizes a gain standard to determine absolute gain as illustrated in the Figure 7. In one set, using the standard gain antenna as the receiving antenna, the received power  $(P_s)_{dBm}$  into a matched load is recorded and it can be derived as

$$(1) : (P_s)_{dBm} = (P_{TR})_{dBm} + (G_s)_{dBi}$$

where  $(P_{TR})_{dBm}$  is transmitted power and  $(G_s)_{dBi}$  is the standard gain antenna. With the maintained geometrical arrangement and transmitted power  $(P_{TR})_{dBm}$ , the standard gain antenna is replaced by the test antenna and the received power  $(P_T)_{dBm}$  into a matched load is recorded. Then, the equation (1) can be stated as

$$(2) : (P_T)_{dBm} = (P_{TR})_{dBm} + (G_T)_{dBi}$$

where  $(G_T)_{dBi}$  is the gain of the test antenna. By substituting equation (1) to (2), it can derive as

$$(3) : (P_s)_{dBm} - (G_s)_{dBi} = (P_T)_{dBm} + (G_T)_{dBi}$$

Subsequently, the value of the antenna gain can be obtained by using equation (4):

$$(4) : (G_T)_{dBi} = (G_S)_{dBi} + [(P_T)_{dBm} - (P_S)_{dBm}]$$

In the array designs, the radiation patterns are measured at the different desired angle. The normalized peak power value of each angle is considered as the received power for the antenna.

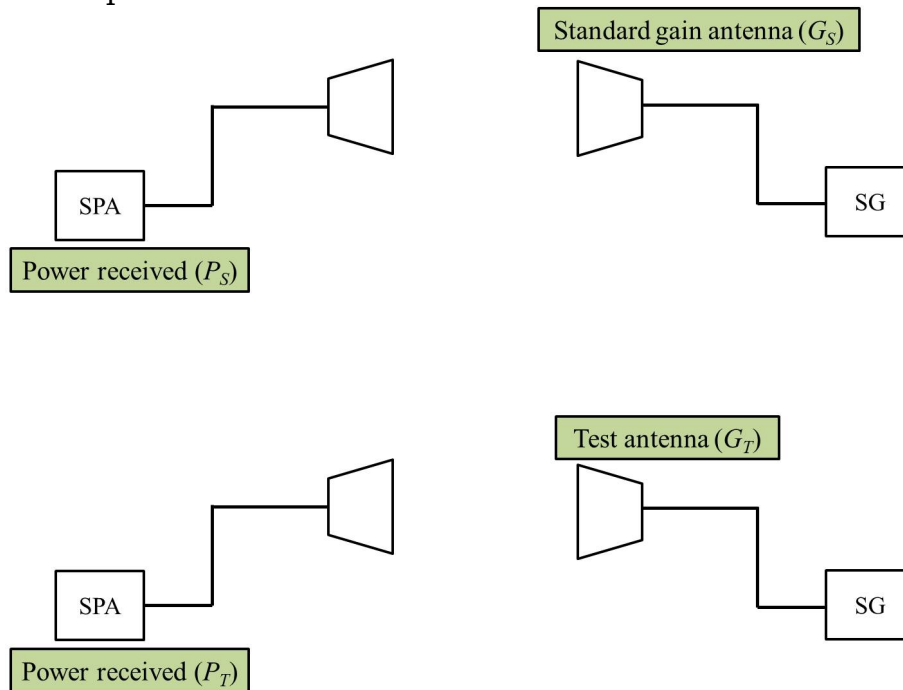


**Figure 7:** The block diagram of gain-transfer method

## 5.0 Result

This section will be presented the verification of the fabricated antenna. The simulated and measured results are also compared.

### 5.1 Single element DRA

The single element DRA excited in the  $TE_{163}^y$  mode (Shahadan et al, 2017) was fabricated and its photograph is as shown in Figure 8. The measured reflection coefficients in Figure 9 depict that there is a slight shift in the resonant frequency due to the fabrication tolerance as much as +0.05 mm for  $w$ ,  $d$  and  $h$  as shown in Figure 10. The antenna with a ground plane size of  $1\lambda$  was measured and the results are consistent with the simulated results. Note that the simulated and measured 10-dB impedance bandwidths are 2.7 GHz (18%) and 2.5 GHz (17.2%), respectively. Although the difference is very minimal, at only 0.8% of the  $TE_{163}^y$  mode, but it is still acceptable and comply with the targeted enhanced bandwidth.

The normalized radiation patterns are then compared as illustrated in Figure 11. Almost identical patterns are observed between the simulated model and the normalized measured patterns, especially in the  $H$ -plane. A spacing of  $s = 0.46\lambda$ , produces a good compromise between the beamwidth and sidelobe levels. Besides that, the measured gain for the DRA excited in  $TE_{163}^y$  mode has achieved 9.76 dBi in comparison to 9.95 dBi from the simulated.

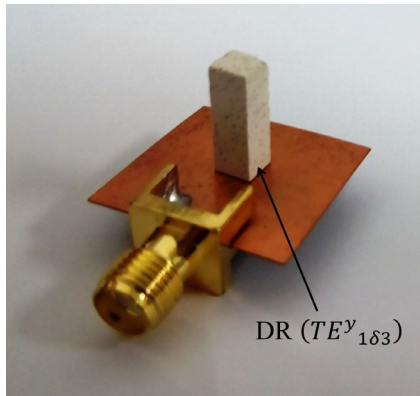


**Figure 8:** 3D view of fabricated single element DRA

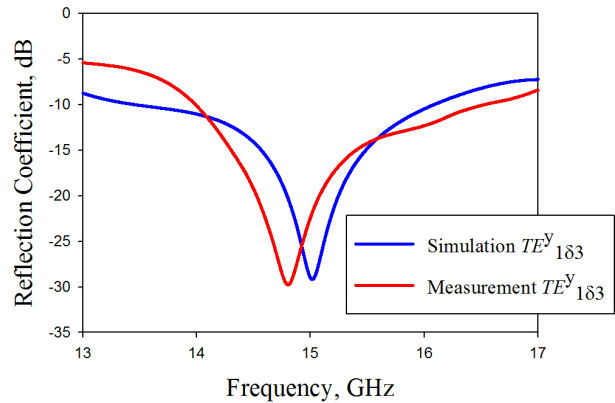


**Figure 9:** Reflection coefficients of the single element DRA



In simulation ( $w = d = 4$  mm)

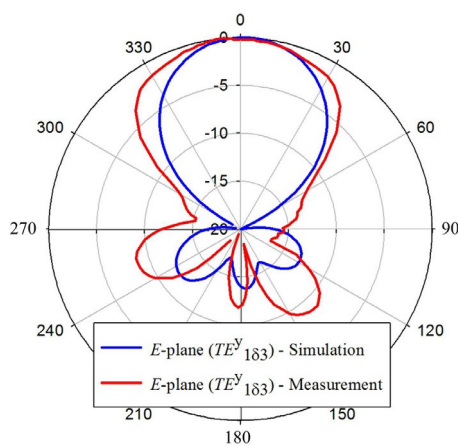
(a)



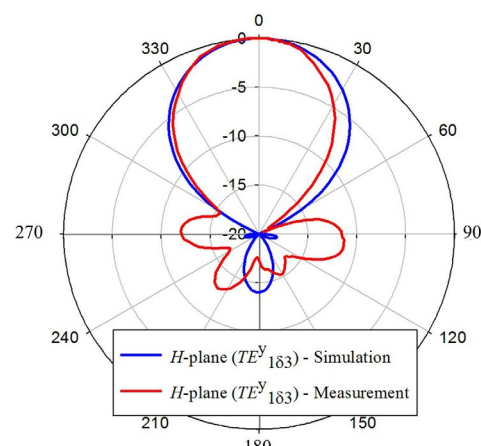
In simulation ( $h = 11.5$  mm)

(b)

**Figure 10:** Verification dimension of fabrication (a)  $w$  and  $d$  (b)  $h$



(a)



(b)

**Figure 11:** Radiation pattern of the single element DRA excited in the higher order mode,  $TE^y_{183}$  at 15 GHz

## 5.2 Switchable DRA subarray (3-elements)

The switchable DRA subarray with switching configuration (Shahadan et al, 2017) was fabricated as shown in Figure 12. The measured reflection coefficient reactions at different switching angles are depicted in Figure 13.

It can be perceived that there is a slight difference in the simulated and measured reflection coefficient at different switching angle. However, by connecting the port directly to the VNA, the results of the reflection coefficient showed that the losses for five various switching angles have been reduced in the range of 2 to 3 dB. Meanwhile, the switchable DRA array has produced acceptable measured gain which are 8.45 dBi, 8.95 dBi, 8.85 dBi, 9.25 dBi and 9.15 dBi at  $0^\circ$ ,  $-19^\circ$ ,  $+19^\circ$ ,  $-32^\circ$  and  $+32^\circ$ , respectively.

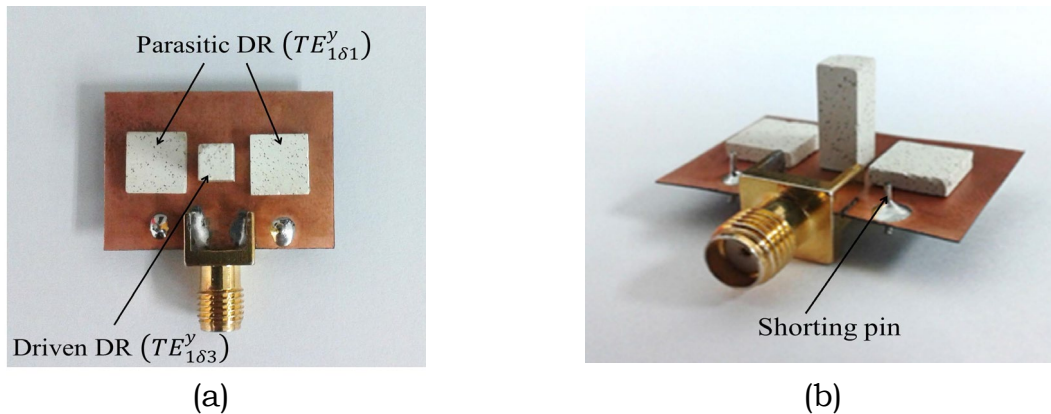


**Figure 12:** A prototype of the fabricated DRA (a) Top view (b) 3D view

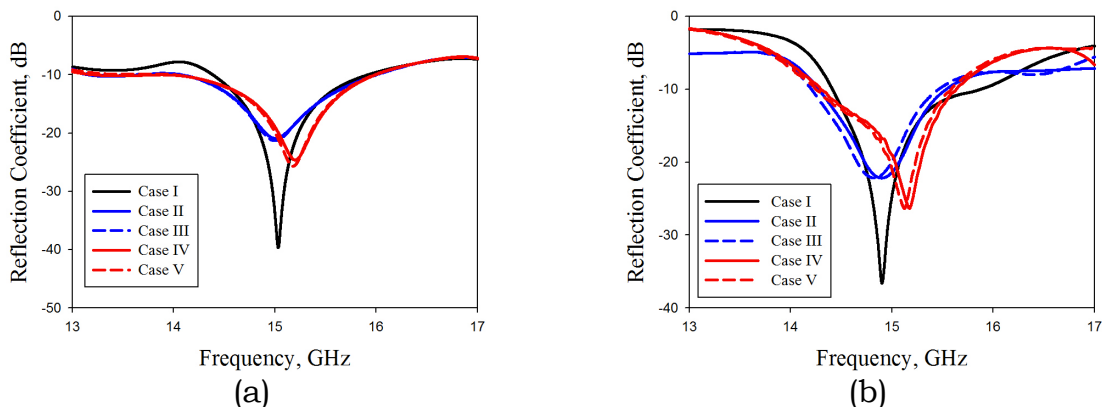


**Figure 13:** Reflection coefficient of various angle (a) Simulated and (b) Measured

### 5.3 High gain switchable DRA array (6-elements)

From the analysis that has been performed and discussed in the previous section, the next concern is on the verification of the proposed high-gain switchable DRA array. Figure 14 shows the fabricated prototype of the proposed high-gain switchable DRA array with switched-line phase shifter (Shahadan et al, 2018). The reflection coefficients performances at different cases are then practically measured by using a vector network analyzer (VNA). Afterward, the comparison is made between the simulated and measured results. The findings show that the measured reflection coefficients for all cases were less than -10 dB with a slight difference in the simulated and measured bandwidth. This is maybe due to the fabrication tolerance of the feeding network and DRs. Besides that, the soldered copper thickness also has a significant effect to the measurement result which is not included during the simulation. However, the observed differences between the simulated and measured bandwidth were in the range of 0.1 to 0.6 GHz only with the average bandwidth of 2.6 GHz.

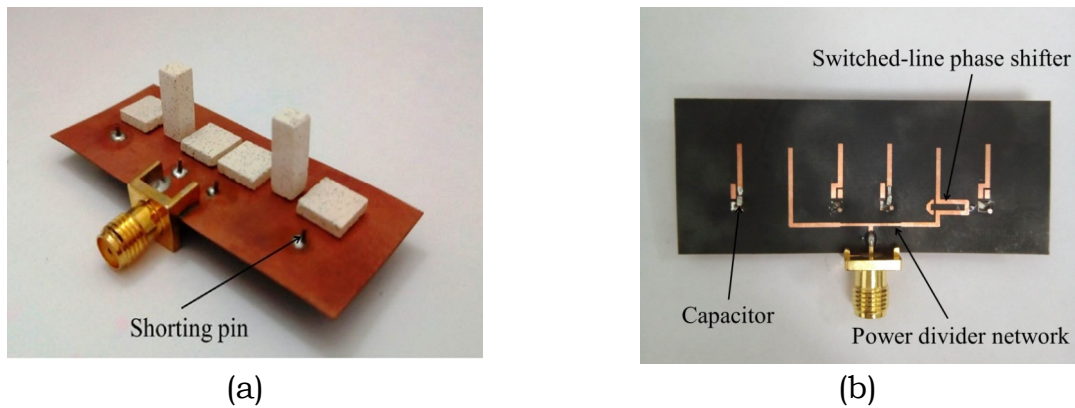


**Figure 14:** A prototype of the fabricated high-gain switchable DRA array (a) 3D View (b) Back View

Capability of the switchable beam at  $H$ -plane was observed for three various cases as presented in Figure 15. It is clearly indicated that the measured beam was able to switch approximately with the simulated beam at  $0^\circ$ ,  $-30^\circ$ ,  $+30^\circ$ . In this regard, a change in main beam radiation angle was achievable by switching the switched-line phase shifter and the termination capacitor on the parasitic element. Although the measured gain for all cases is slightly reduced from the simulated results, it has achieved more than 12 dBi as required in the 5G applications with the HPBW of less than  $30^\circ$ .

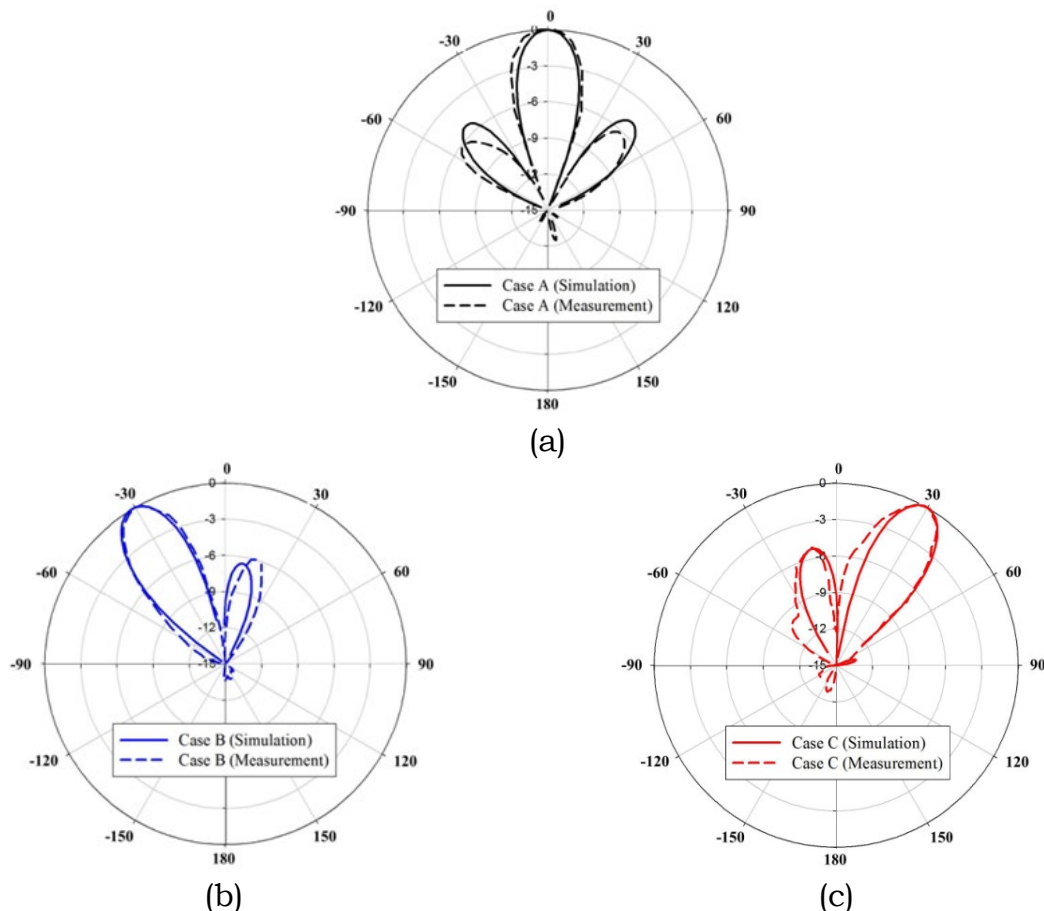


**Figure 15:** Simulated and measured normalized beam pattern for various cases of the high gain DRA array (a) Case A at  $0^\circ$  (b) Case B at  $-30^\circ$  (c) Case C at  $+30^\circ$

## 6.0 Conclusion

The fabrication, measurement and verification process of switchable dielectric resonator antenna array for 5G applications has been presented. The result has clearly indicated the better performance achieved from the proposed technique compared to the conventional technique. Besides, the misalignment between the DR and the feeding network is also minimized. Furthermore, the final design which is high gain switchable DRA array has accomplished the desired steering angle by switching the capacitor loading and the integrated switched-line phase shifter without using any external phase shifter. More importantly, the proposed design not only contributes in reducing the number of antenna elements, but it has also achieved the best switching angle at  $\pm 30$  degrees by using only 2 ports that are capable to cover  $60^\circ$  sector. It can be considered that this proposed switchable DRA array can be potentially applied for 5G applications.

## References

- Abdallah, M., Wang, Y., Abdel-Wahab, W. M. and Safavi-Naeini, S. (2017) Design and optimization of SIW center fed series rectangular dielectric resonator antenna (DRA) array with 45 linear polarization. *IEEE Transactions on Antennas and Propagation*, 88, 1–1. <https://doi.org/10.1109/TAP.2017.2768569>
- Ahmed, B., Saleem, I., Zahra, H., Khurshid, H. and Abbas, S. M. (2012) Analytical study on effects of substrate properties on the performance of microstrip patch antenna. *International Journal of Future Generation Communication and Networking*, 5, 113–122.
- Balanis, C. A. (2005). *Antenna theory* (3rd ed.). Hoboken, New Jersey: Wiley-Interscience.
- Boccardi, F., Heath, R. W., Lozano, A., Marzetta, T. L., & Popovski, P. (2014). Five disruptive technology directions for 5G. *IEEE Communications Magazine*, 52(2), 74-80.
- Nor, N. A, Jamaluddin, M. H., Kamarudin, M. R., and Khalily, M. (2016). Rectangular dielectric resonator antenna array for 28 GHz applications. *Progress in Electromagnetics Research C*, 63, 53-61.
- Pi, Z and Khan, F. (2011). An introduction to millimeter-wave mobile broadband systems. *IEEE Communications Magazine*, 49(6), 101-107. June 2011.
- Rogers Corporation, (2016) *RT/duroid® 5870 /5880 High Frequency Laminates*, Retrieved on August 8, 2019. From <https://www.rogerscorp.com/documents/606/acs/RT-duroid-5870-5880-Data-Sheet.pdf>.

Shahadan, N. H., Kamarudin, M. R., Zainal, N. A., Nasir, J., Khalily, M., Jamaluddin, M. H. (2015) Investigation on feeding techniques for rectangular dielectric resonator antenna in higher-order mode for 5g applications. *Applied Mechanics and Materials*, 781, 41-44. <https://doi.org/10.4028/www.scientific.net/AMM.781.41>

Shahadan, N. H., Jamaluddin, M. H., Kamarudin, M. R. and Yamada, Y. (2017). Higher-order mode rectangular dielectric resonator antenna for 5G Applications, *Indonesian Journal of Electrical Engineering and Computer Science*, 5(3), 584–592.

Shahadan, N. H., Jamaluddin, M. H., Kamarudin, M. R., Yamada, Y., Khalily, M., Jusoh, M., Dahlan, S. H. (2017). steerable higher-order mode dielectric resonator antenna with parasitic elements for 5g applications, *IEEE access*, 5, 22234-22243. <https://doi.org/10.1109/ACCESS.2017.2760924>

Shahadan, N. H., Jamaluddin, M. H., Dahri, M. H., Kamarudin, M. R., and Yusof, K. H. (2018) *High gain switchable dielectric resonator antenna array for 5g applications*, 2018 International Symposium on Antennas and Propagation (ISAP), Busan, Korea, 1-2.

Wang, C-X., Haider, F., Gao, X., You, X-H., Yang, Y., Yuan, D., Hepsaydir, E. (2014). Cellular architecture and key technologies for 5G wireless communication networks. *IEEE Communications Magazine*, 52(2), 122-130. <https://doi.org/10.1109/MCOM.2014.6736752>

Yusuf, Y., & Gong, X. (2008). A low-cost patch antenna phased array with analog beam steering using mutual coupling and reactive loading. *IEEE Antennas and Wireless Propagation Letters*, 7, 81-84. <https://doi.org/10.1109/LAWP.2008.916689>